

Orbital order and fluctuations in the two-leg ladder materials BaFe_2X_3 ($X = \text{S}$ and Se) and CsFe_2Se_3

Kou Takubo,* Yuichi Yokoyama, and Hiroki Wadati

Institute for Solid State Physics, University of Tokyo, Kashiwa, Chiba 277-8581, Japan

Shun Iwasaki and Takashi Mizokawa

Department of Applied Physics, Waseda University, Okubo 169-8555, Japan

Teak Boyko, Ronny Sutarto, and Feizhou He

Canadian Light Source, Saskatoon, Saskatchewan S7N 2V3, Canada

Kazuki Hashizume, Satoshi Imaizumi, Takuya Aoyama, Yoshinori Imai, and Kenya Ohgushi

Department of Physics, Tohoku University, Sendai 980-8578, Japan

(Received 17 April 2017; revised manuscript received 15 September 2017; published 27 September 2017)

The electronic structure of BaFe_2X_3 ($X = \text{S}$ and Se) and CsFe_2Se_3 in which two-leg ladders are formed by the Fe sites are studied by means of x-ray absorption and resonant inelastic x-ray scattering spectroscopy. The x-ray absorption spectra at the Fe L edges for BaFe_2X_3 exhibit two components, indicating that itinerant and localized Fe $3d$ sites coexist. Substantial x-ray linear dichroism is observed in polarization dependent spectra, indicating the existence of orbital order or fluctuation in the Fe ladder even above the Néel temperature T_N . Direct exchange interaction along the legs of the Fe ladder stabilizes the orbital and antiferromagnetic orders in BaFe_2S_3 , while the ferromagnetic molecular orbitals are realized between the rungs in CsFe_2Se_3 .

DOI: [10.1103/PhysRevB.96.115157](https://doi.org/10.1103/PhysRevB.96.115157)**I. INTRODUCTION**

The magnetic-orbital fluctuations and their anisotropies in iron-based superconductors have been attracting much attention. The parent compounds of the iron-based superconductors show antiferromagnetic (AF) transitions at low temperatures, typically exhibiting striped-type magnetic ordering [1–3]. On the basis of theoretical analyses on multiband models with hole and electron Fermi pockets, the striped-type magnetic ordering is stabilized by Fermi-surface nesting, and the associated AF and orbital fluctuations are proposed to induce the superconductivity [3–8]. However, there are some iron-based superconductors showing significant disagreement with the Fermi-surface nesting scenario. For example, superconductivity with $T_c \sim 30$ K in 245 system ($\text{A}_2\text{Fe}_4\text{Se}_5$, $A = \text{K}$, Rb , and Cs) [9–11] appears in the vicinity of the Mott insulating state with block-type AF ordering. In this context, it is very important to study the nature of the Mott insulating state in the parent compounds of iron-based superconductors.

Recently, another insulating Fe chalcogenide AFe_2X_3 ($A = \text{Cs}$ and Ba , $X = \text{S}$ and Se) has been attracting attention due to the specific quasi-one-dimensional crystal structure and magnetism [12–27]. In this family of compounds, $\text{Fe}(\text{S},\text{Se})_4$ tetrahedra share their edges and form a two-leg ladder of Fe sites as shown in Fig. 1(a). These compounds all exhibit unique magnetic ordering. The magnetic structure of BaFe_2S_3 ($Pnma$ space group) is a one-dimensional analog of the block magnetism observed in $\text{A}_2\text{Fe}_4\text{Se}_5$, in that four Fe spins in the two-leg ladder form a ferromagnetic block and the neighboring blocks are antiferromagnetically coupled as illustrated in Fig. 1(f) [13–16]. In contrast, the magnetic structures of

BaFe_2S_3 and CsFe_2Se_3 ($Cmcm$ space group) are of the stripe type, in which the magnetic moments couple ferromagnetically along the rung and antiferromagnetically along the leg direction [17,18]. However, the magnetic moments in CsFe_2Se_3 point toward the layers, while those in BaFe_2S_3 point toward the rungs.

Moreover, recent works under high pressures revealed that BaFe_2S_3 , which is the most conductive compound among these compounds, shows an appearance of the superconducting phase at $T_c \sim 14$ K under 11 GPa without major crystal structure change [19]. Also it has been clarified that the superconducting phase is in the vicinity of bandwidth-control type Mott transition [20]. In addition, the magnetic transition temperature and resistivity of BaFe_2X_3 (Fe^{2+}) depend on the sample stoichiometry. Lei *et al.* reported the activation-type temperature dependence for BaFe_2Se_3 with a band gap of 0.18 eV [21]. On the other hand, one-dimensional variable range hopping was reported, indicating that some carriers are localized due to strong scattering effects in the quasi-one-dimensional structure [16,20,22]. Moreover, coexistence of the itinerant and localized electrons was indicated by the resonant inelastic x-ray scattering (RIXS) [23] and x-ray photoemission spectroscopy (XPS) [24]. These observations suggest that the itinerant electrons introduced by small Fe vacancies or some other effects would be responsible for the variable range-hopping behavior of the resistivity [16,20,22]. In contrast to BaFe_2X_3 , CsFe_2Se_3 with formal Fe valence of +2.5 is much more insulating. Usually, Mott insulators with integer number of valence are expected to be more insulating than the mixed valence systems. Such puzzling mismatch between the formal valence and the transport behavior indicates unusual electronic states in the vicinity of the superconducting phase of AFe_2X_3 . The x-ray linear dichroism (XLD) for x-ray absorption spectroscopy (XAS) and RIXS are

*ktakubo@issp.u-tokyo.ac.jp

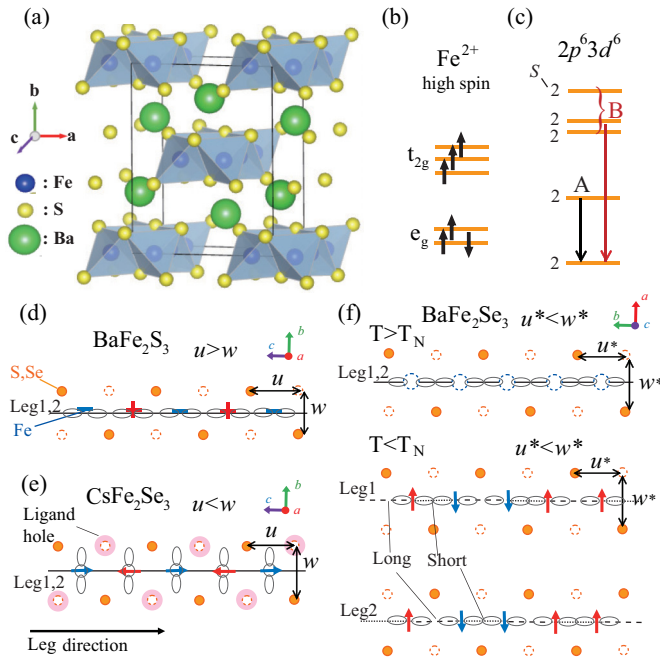


FIG. 1. Crystal and electronic structure of BaFe₂X₃ and CsFe₂Se₃. (a) Crystal structure of BaFe₂S₃ visualized using the software package VESTA [28]. (b) Electronic configuration of Fe²⁺ high-spin state in a tetrahedral symmetry. (c) Multiplet levels of the initial state for 2p⁶3d⁶ suggested in Ref. [23]. The Coulomb and crystal field interactions are considered with associated *S* number. A and B mark the two dominant *d-d* excitation peaks seen in the RIXS experiment. (d),(e),(f) Schematic drawing of the magnetic structure and lattice distortion in a leg of Fe ladder for (d) BaFe₂S₃, (e) CsFe₂Se₃, and (f) BaFe₂Se₃, viewed from a side of the ladder. The definitions of crystal axes are different between BaFe₂S₃, CsFe₂Se₃, and BaFe₂Se₃. The S or Se layers locate up (solid circle) and down (dotted circle) the Fe-leg layer and consist of Fe(S,Se)₄ tetrahedra. Gray lobes indicate examples of occupied orbitals. Magenta shades in (e) indicate the ligand holes suggested in Ref. [24].

ideal tools to detect electronic anisotropy in such systems with charge and orbital degrees of freedom of transition-metal 3*d* electrons.

In other families of the iron-based superconductors, 122 (AFe₂As₂, A = alkaline-earth) and 1111 (RFeAsO, R = rare earth) systems, the Néel temperature (*T_N*) and structural transitions (*T_S*) are split, which have recently been considered as a manifestation of electronic nematic order [29]. These orders have been inferred from the unusual anisotropy in resistivity [30–32], optical conductivity [33], and orbital occupancy [34,35] observed at the temperatures above *T_S* and *T_N*. In the present paper, we investigate the electronic structure of BaFe₂S₃, BaFe₂Se₃, and CsFe₂Se₃ in the Fe sites by means of XAS and RIXS at the Fe *L*_{2,3} absorption edges. An opposite XLD, namely the electronic anisotropy, is observed for BaFe₂X₃ and CsFe₂Se₃ at room temperature, indicating the existence of the orbital order or fluctuation above *T_N*. The orbital and AF order along the legs of Fe ladder is emerged via the direct exchange interaction between the Fe sites in BaFe₂S₃. On the other hand, the molecular orbital formation along the rung is associated in CsFe₂Se₃.

II. EXPERIMENT

Single crystals of BaFe₂S₃, BaFe₂Se₃, and CsFe₂Se₃ were grown by the melt-growth method [17,22]. XAS and RIXS measurements were performed at the REIXS beamline of the Canadian Light Source [36]. The single crystals were cleaved at room temperature (300 K) under the base pressure of 5×10^{-6} Pa for the XAS and RIXS measurements. The cleaved surfaces were oriented to the (110) planes for BaFe₂S₃ and CsFe₂Se₃, and (100) plane for BaFe₂Se₃, parallel to the legs of ladder. Although the crystals of BaFe₂Se₃ consist of some blocks misaligned by a rotation along the ladder direction [13,23], this fact does not seriously affect the main conclusion of XLD for *E*//leg or *E* ⊥ leg discussed later. The XAS spectra were recorded both in the total-electron-yield (TEY) and total-fluorescence-yield (TFY) modes. At the RIXS measurement, the samples were measured at the incident angle of 60° and the emissions were detected at $\theta = 90^\circ$ for the x ray [see inset of Fig. 5(d) about the experimental geometry]. The beamline slit was set to 25 μm, which resulted in an effective combined resolution of both the incoming beam and spectrometer of ~0.8 eV for RIXS measurements at the Fe *L*₃ edge. The energy of outgoing photons was calibrated by a reflection from a copper plate.

III. RESULTS AND DISCUSSION

Figure 2 shows the XAS spectra at the Fe *L*_{2,3} absorption edge of BaFe₂S₃, BaFe₂Se₃, and CsFe₂Se₃ taken with the (a) TEY and (b) TFY modes at room temperature. Spectral difference between the less-distorted TEY and bulk-sensitive TFY spectra is barely observed, indicating the clean ordered surface for these samples. The two white lines in the spectra result from 2*p* to 3*d* dipole transitions (2p⁶3d⁶ → 2p⁵3d⁷) with the well-separated spin-orbit-split 2*p* states 2p_{3/2} (*L*₃) and 2p_{1/2} (*L*₂), appearing respectively at around ~708 and ~721 eV. No sharp multiplet is observed in the spectra that exhibits a similar spectral shape as Fe chalcogenides of Fe(S,Te) [37] and Fe-pnictide materials [35,38–41]. Additionally, some spectral weights can be seen in the energy range of 3–5 eV above the white lines. These features are an indication of interaction of the chalcogen sites with the Fe 3*d* states [37] and is notably well separated in the sharp spectrum for CsFe₂Se₃, which are indicated in the red arrows in Fig. 2(a). Despite the formal Fe valence of +2.5 for CsFe₂Se₃, the spectrum of CsFe₂Se₃ is very sharp but consistent with the observation of a previous Fe 2*p* XPS study [24], indicating a localized Mott insulating nature with Fe²⁺. If all the Fe sites in CsFe₂Se₃ take the high-spin Fe²⁺ configuration, the extra positive charge (+0.5 per Fe) should be located at the Se sites. Since the charge-transfer energy from Se 4*p* to Fe 3*d* is small, if Fe³⁺ exists in CsFe₂Se₃, it should take the *d*⁶ \bar{L} configuration instead of *d*⁵ [24]. In this ligand hole picture, the two-leg ladder in CsFe₂Se₃ accommodates the *d*⁶-like and *d*⁶ \bar{L} -like sites. Assuming that the *d*⁶-like and *d*⁶ \bar{L} -like sites are aligned along the rung, the Se 4*p* hole should be located at the Se sites sandwiched by the two legs as schematically shown in Fig. 1(e).

On the other hand, some shoulder structures below the white lines are observed in the spectra of BaFe₂S₃ and BaFe₂Se₃, that

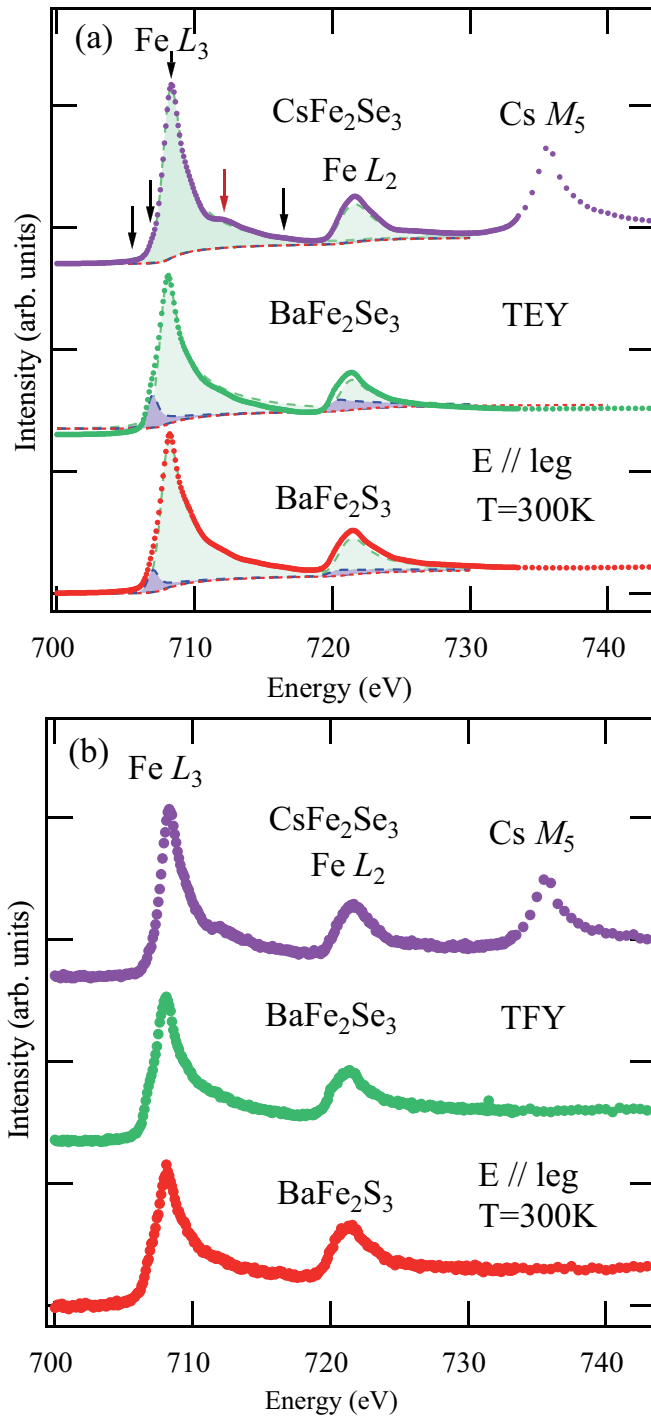


FIG. 2. XAS spectra at the Fe $L_{2,3}$ edges for BaFe_2X_3 ($X = \text{S}$ and Se) and CsFe_2Se_3 taken in the (a) TEY and (b) TFY modes. The dashed lines indicate the results of curve fitting. The arrows indicate the incident energies used in the RIXS measurements shown in Fig. 5.

are also similar to the Fe $2p$ XPS spectra and corresponding to rather electron doping compared to the case of CsFe_2Se_3 . In Fig. 2(a), the results of Mahan's-line shape fitting are indicated by the dashed curves. The weak but significant components are observed at the pre-edge region ~ 1.0 eV below the white lines for BaFe_2Se_3 and BaFe_2S_3 . On the XPS study, these two components have been ascribed as the contribution from

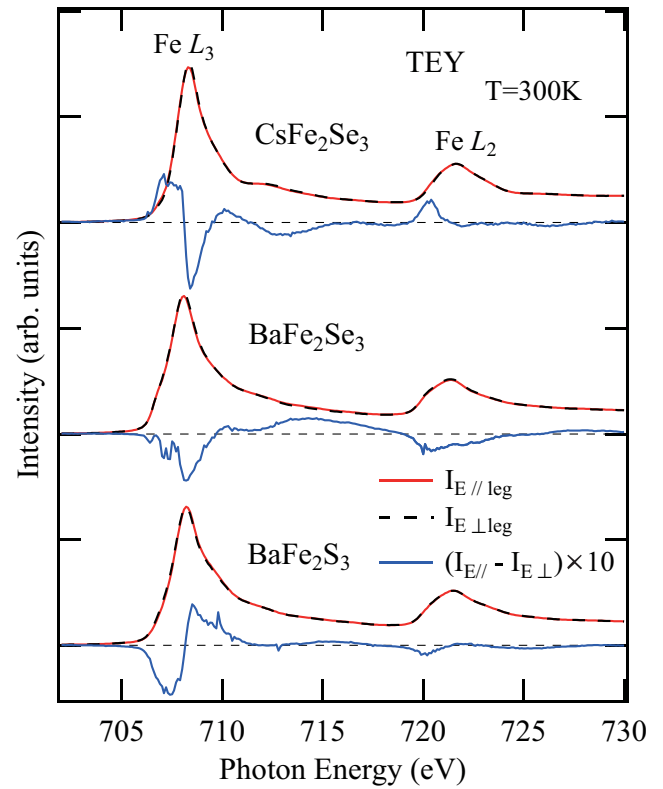


FIG. 3. XAS spectra at the Fe $L_{2,3}$ edges with two different polarizations taken in the TEY modes at $T = 300$ K for BaFe_2X_3 ($X = \text{S}$ and Se) and CsFe_2Se_3 . The blue curves are the XLD spectra.

itinerant and localized electrons. Since the pre-edge region of XAS for transition-metal $L_{2,3}$ edges corresponds to the transition to unoccupied d state near the Fermi level, these low energy structures originate from the itinerant e_g empty state of the Fe^{2+} high-spin state [see Fig. 1(b)]. The itinerant and localized electrons will coexist in BaFe_2Se_3 and BaFe_2S_3 . Namely, self-dopings from the Se $4p$ and S $3p$ to Fe $3d$ states arise from smallness of the charge transfer and cause partial delocalization of the electrons in these systems. On the other hand, the Fe $3d$ electrons with the Fe^{2+} high-spin configuration and the Se $4p$ holes are localized in CsFe_2Se_3 .

In addition to these features, the XAS spectra at the Fe edges exhibit unique anisotropies. Figure 3 gives the XLD spectra of BaFe_2X_3 ($X = \text{S}$ and Se) and CsFe_2Se_3 at room temperature. The spectra are normalized by the area between 700 eV and 718 eV. The substantial XLD ($I_{E//\text{leg}} - I_{E\perp\text{leg}}$) are observed for all samples and exhibit an opposite behavior for BaFe_2X_3 and CsFe_2Se_3 . The sign of XLD is minus for BaFe_2S_3 below the L_3 main peak of 708.1 eV in the overall pre-edge region and plus in the higher energy region. XLD observed in the spectra for BaFe_2S_3 is fairly similar to that obtained for BaFe_2As_2 ($I_{AF} - I_{\text{ferromagnetic}}$) below T_s [35]. XLD for BaFe_2As_2 was consistent with the existence of an orbital order along their AF direction and an opposite to tendency of their local structural distortion of $a_{AF} > b_{\text{ferromagnetic}}$ [35,42]. The spectrum for BaFe_2S_3 in the pre-edge region taken with the $E//\text{leg}$ ($E\perp\text{leg}$) polarization detects the empty e_g state of the $d_{3z^2-r^2}$ ($d_{x^2-y^2}$) orbital as discussed earlier. Here, z is defined to be parallel to the leg direction, or c for BaFe_2S_3 and CsFe_2Se_3 , and b for BaFe_2Se_3 ,

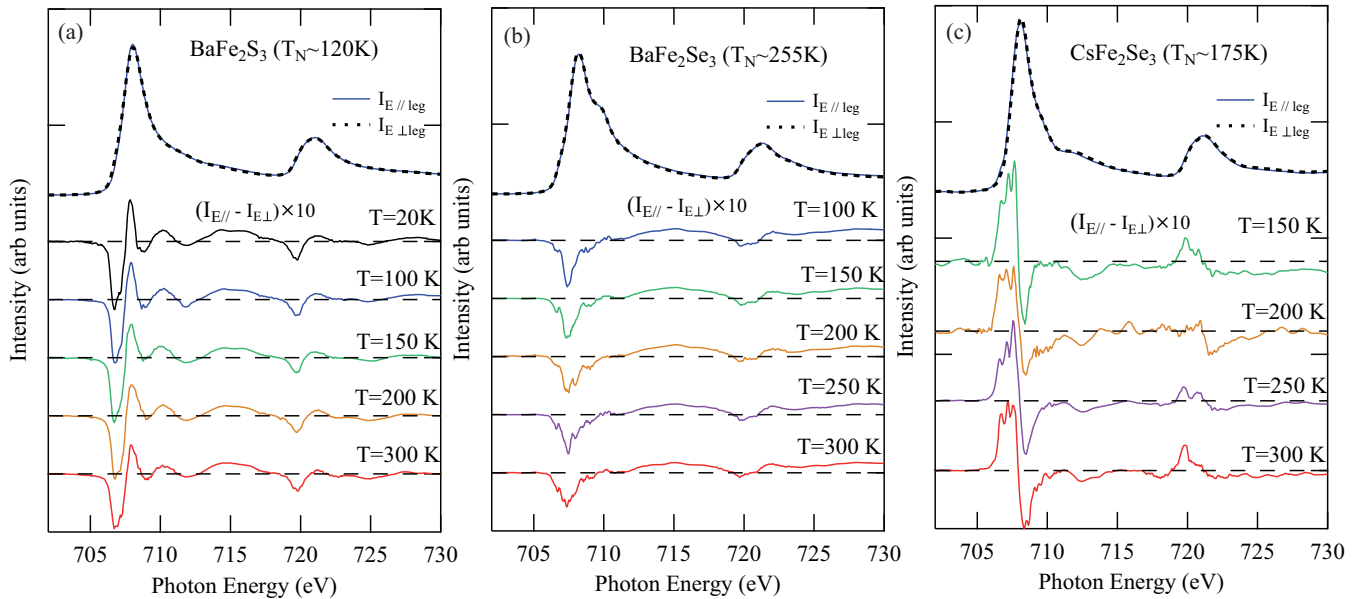


FIG. 4. Temperature dependence of XLD at the Fe $L_{2,3}$ edges in the TEY modes for the different badges of crystals, (a) BaFe_2S_3 , (b) BaFe_2Se_3 , and (c) CsFe_2Se_3 .

respectively. Therefore, $d_{3z^2-r^2}$ will be occupied and the orbital order along the leg direction is indicated in BaFe_2S_3 .

In the case of BaFe_2Se_3 , most of the $d_{3z^2-r^2}$ orbitals should be occupied, since XLD in the pre-edge region of ~ 707 eV is essentially similar to that of BaFe_2S_3 . However, a dip-hump-like shape is observed at the pre-edge region and the sign of XLD is still minus at the main-peak region of ~ 708 eV. Since the crystal of BaFe_2Se_3 has many twins at room temperature compared to BaFe_2S_3 and CsFe_2Se_3 [22], it is possible that the crystal of BaFe_2Se_3 contains many defects. The small Fe vacancy will affect the electronic configuration for BaFe_2Se_3 and the orbital order may become more complicated, corresponding to their block-type magnetism and lattice distortion below T_N .

On the other hand, there is a peak in the pre-edge region of XLD for CsFe_2Se_3 and it exhibits a dip at the main-peak structure around 708.4 eV. Therefore, more holes are suggested in the $d_{3z^2-r^2}$ orbital rather than in the $d_{x^2-y^2}$. Namely, the orbital order perpendicular to the leg direction is indicated in CsFe_2Se_3 , in contrast to BaFe_2S_3 [see also Fig. 1(e)]. However, the very sharp Fe peaks with the satellitelike structures of CsFe_2Se_3 cannot be simply understood for the formal valence of 2.5+ with any kind of the orbital order in the Fe sites, whereas this observation is still consistent with the insulating nature of this compound.

One may consider that the anisotropic spectra discussed above are naturally expected on the basis of their local structural distortions in the two-leg ladder of AFe_2X_3 and do not link to the existence of orbital orders. However, the present tendency of XLD for BaFe_2S_3 is opposite to its local distortion, which was theoretically clarified by Chen *et al.* for BaFe_2As_2 [42]. The local distortions around the Fe sites can be described by the elongation or compression for the FeS_4 tetrahedra. The FeS_4 tetrahedra of BaFe_2S_3 are elongated along the leg direction ($u/w \sim 1.03$) [12] [see Fig. 1(d)], which corresponds to the AF direction for BaFe_2As_2 . In this

case, the diplike structure would be observed in XLD of the higher energy region and hump would be observed in the lower energy region of the Fe L_3 edge [42]. However, the observed XLD for BaFe_2S_3 is opposite to these tendencies. On the other hand, the FeSe_4 tetrahedra of CsFe_2Se_3 are compressed ($u/w \sim 0.98$) along the leg [17]. Moreover, the orbital order in many iron-based superconductors including BaFe_2As_2 were unable to be reproduced by simple first-principle calculations based on the structural data and still has been a controversial problem. Actually, a recent first-principle calculation for paramagnetic metallic state of BaFe_2S_3 indicates the different orbital filling in the Fe 3d states ($n_{d_{x^2-y^2}} > n_{d_{3z^2-r^2}}$) [43,44]. Therefore, the observed XLD for BaFe_2S_3 and CsFe_2Se_3 cannot be explained from their structural distortions, indicating the existence of orbital order or fluctuation at room temperature.

Furthermore, the tendency of XLD in the lower energy region of the Fe L edges show scarcely any temperature dependence as shown in Fig. 4. While the higher energy structures of L_3 around ~ 709 eV show some cleavage dependences owing to the defects and/or contaminations, the tendency and magnitude of XLD are essentially similar to those obtained at Fig. 3. As the temperature decreases, the magnitudes of XLD for all samples steadily increase but irrelevant to T_N . Those for BaFe_2S_3 and BaFe_2Se_3 at $T = 100$ K (and $T = 200$ K) are $\sim 30\%$ (and $\sim 10\%$) larger than those at $T = 300$ K. On the other hand, that for CsFe_2Se_3 at $T = 150$ K (and $T = 200$ K) is $\sim 30\%$ (and $\sim 0\%$) larger than that at $T = 300$ K. Therefore, the present temperature dependence of XLD strongly supports the scenario of the orbital order or fluctuation in these systems even above T_N .

In order to examine the energy levels in the Fe sites with unique anisotropies discussed above, polarization dependent RIXS spectra have been acquired for incident energies $h\nu_i$ across the Fe L_3 -edge XAS spectra as indicated by the arrows in Fig. 2(a). The data are shown in Fig. 5 for (a) BaFe_2S_3 ,

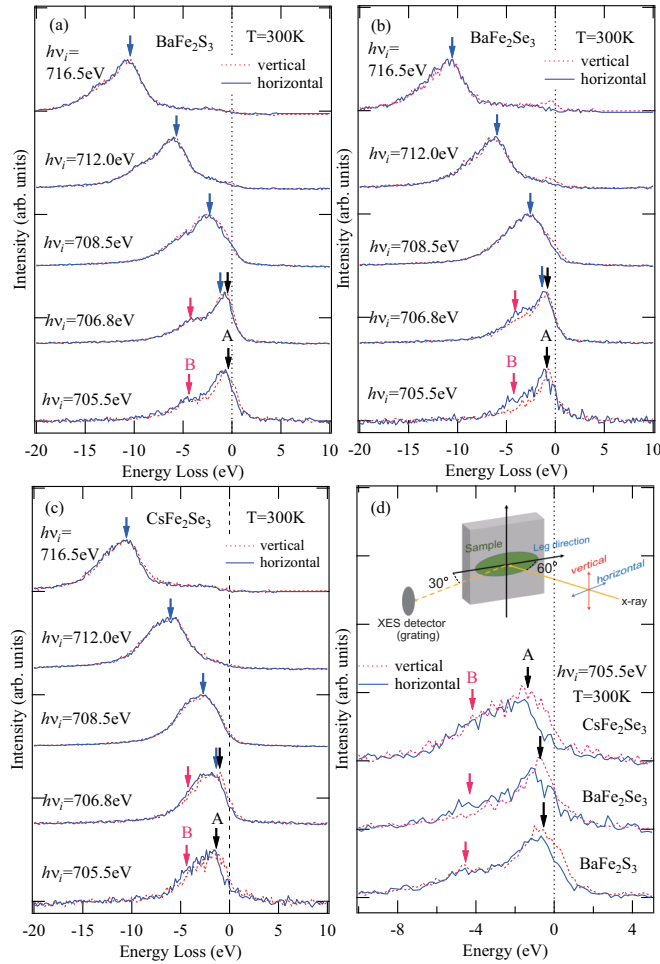


FIG. 5. RIXS spectra measured with selected incident energies at the Fe L_3 edge for (a) BaFe_2S_3 , (b) BaFe_2Se_3 , and (c) CsFe_2Se_3 at $T = 300$ K. The blue arrows indicate the contribution from the fluorescence. The black and red arrows indicate Raman-like peaks labeled as A and B. (d) RIXS spectra with $h\nu = 705.5$ eV, zoomed into the low-energy-loss region. The inset shows the experimental geometry of RIXS.

(b) BaFe_2Se_3 , and (c) CsFe_2Se_3 , respectively, on an energy loss scale $\hbar\Omega = h\nu_f - h\nu_i$, where $h\nu_f$ is the energy of outgoing photons. Although some elastic lines are observed at zero energy loss taken with the vertical polarization, these are barely observed on the spectra with horizontal polarization owing to the experimental geometry given in the inset of Fig. 5(d). The strong fluorescence indicated by the blue arrows are observed on the spectra with $h\nu_i > 706.8$ eV and disperses from 1 eV energy loss to higher energy losses, which was ascribed by the hybridization effects between Fe $3d$ states and Se $4p$ states in the high-resolution study for BaFe_2Se_3 by Monney *et al.* [23]. The fluorescence contributions shift to higher energy losses for increasing incident energies, as fluorescence in RIXS typically occurs at fixed x-ray emission energy. Monney *et al.* also suggested two Raman-like peaks labeled as A and B, not moving in energy position with variation of incident photon energy, superimposed on top of the fluorescence, which are clearly seen in the spectra with $h\nu_i = 705.5$ eV zoomed in Fig. 5(d). These two Raman-like peaks A and B

corresponding to the energy of $d-d$ excitations in the Fe sites [see Fig. 1(c)]. The peak energies of A roughly correspond to the magnitude of band gap and increase in going from 0.4 eV for BaFe_2S_3 , 0.8 eV for BaFe_2Se_3 , to 1.3 eV for CsFe_2Se_3 , which are more or less consistent with the order for the activation energies [21,22] and threshold energies of the photoemission spectroscopy [24].

The relatively large band gap observed in RIXS and orbital order along the rung direction clarified by XLD for CsFe_2Se_3 can be explained by the molecular orbital formation between the two Fe sites of the rung, namely ferromagnetic dimer formation [45,46]. In this scenario, the bonding orbital accommodates two electrons of the e_g states in the two Fe sites across the rung in CsFe_2Se_3 , and the gap is opened between the bonding and antibonding states. Since the $d_{x^2-y^2}$ orbitals along the rung become a bonding localized state, the $d-d$ excitation of A on RIXS with the vertical polarization and $I_{E//\text{leg}}$ of the pre-edges on XLD are enhanced. On the other hand, the ferromagnetic dimers are destabilized partially in BaFe_2Se_3 and completely in BaFe_2S_3 and then $I_{E\perp\text{leg}}$ of XLD are enhanced. The gap sizes depend on the transfer between the dimers and therefore become very small in BaFe_2X_3 . This scenario seems to be consistent with a recent inelastic neutron scattering study for BaFe_2S_3 [47]. It indicates a strong intraladder ferromagnetic exchange interaction along the rung direction, although BaFe_2S_3 still exhibits the commonly striped AF spin excitations. In addition, the importance of Hund's rule coupling has generally been suggested in iron-based superconductors, which leads to ferromagnetic interaction between the itinerant electrons and local moments [48].

IV. SUMMARY

We have studied the electronic structures of BaFe_2X_3 ($X = \text{S}$ and Se) and CsFe_2Se_3 using x-ray absorption and resonant inelastic x-ray scattering spectroscopy. XAS peak structure at the Fe L edges consists of the two components in BaFe_2X_3 , indicating that the itinerant and localized Fe $3d$ electrons coexist. On the other hand, the sharp peak at the Fe L edges for CsFe_2Se_3 exhibit the single component accompanied with the well separated charge-transfer-like satellite. The distinct electronic anisotropies in the Fe $3d$ states are inferred from the XLD spectra. Different types of the orbital order or fluctuation exist in BaFe_2X_3 and CsFe_2Se_3 even at room temperature far above T_N , which originate from the direct exchange between the $d_{3z^2-r^2}$ orbitals and molecular orbital formation bridging the rungs, respectively. The similarity between these findings and the electronic nematic order observed in other families of the iron-based superconductors having square lattices suggests that the similar exotic phases can be realized in the quasi-one-dimensional structure.

ACKNOWLEDGMENTS

The authors thank Dr. D. Ootsuki and Dr. Y. Hirata for valuable discussions. Research described in this paper was performed at the Canadian Light Source, which is supported by the Canada Foundation for Innovation, Natural Sciences and Engineering Research Council of Canada, the University

of Saskatchewan, the Government of Saskatchewan, Western Economic Diversification Canada, the National Research Council Canada, and the Canadian Institutes of Health Research. This work was supported by the Japan Society for the Promotion of Science (JSPS) of Grant-in-Aid for

Young Scientists (B) (Grant No. 16K20997) and for Scientific Research (B) (Grant No. 16H04019). This work was also partially supported by Ministry of Education, Culture, Sports, Science, and Technology of Japan (X-ray Free Electron Laser Priority Strategy Program) and Mitsubishi Foundation.

-
- [1] Q. Huang, Y. Qiu, W. Bao, M. A. Green, J. W. Lynn, Y. C. Gasparovic, T. Wu, G. Wu, and X. H. Chen, *Phys. Rev. Lett.* **101**, 257003 (2008).
- [2] C. de la Cruz, Q. Huang, J. W. Lynn, J. Li, W. Ratcliff II, J. L. Zarestky, H. A. Mook, G. F. Chen, J. L. Luo, N. L. Wang, and P. Dai, *Nature (London)* **453**, 899 (2008).
- [3] P. Dai, *Rev. Mod. Phys.* **87**, 855 (2015).
- [4] I. I. Mazin, D. J. Singh, M. D. Johannes, and M. H. Du, *Phys. Rev. Lett.* **101**, 057003 (2008).
- [5] K. Kuroki, S. Onari, R. Arita, H. Usui, Y. Tanaka, H. Kontani, and H. Aoki, *Phys. Rev. Lett.* **101**, 087004 (2008).
- [6] C.-C. Lee, W.-G. Yin, and W. Ku, *Phys. Rev. Lett.* **103**, 267001 (2009).
- [7] Y. Yamakawa, S. Onari, and H. Kontani, *Phys. Rev. X* **6**, 021032 (2016).
- [8] A. V. Chubukov, M. Khodas, and R. M. Fernandes, *Phys. Rev. X* **6**, 041045 (2016).
- [9] J. Guo, S. Jin, G. Wang, S. Wang, K. Zhu, T. Zhou, M. He, and X. Chen, *Phys. Rev. B* **82**, 180520 (2010).
- [10] Z. Shermadini, A. Krzton-Maziopa, M. Bendele, R. Khasanov, H. Luetkens, K. Conder, E. Pomjakushina, S. Weyeneth, V. Pomjakushin, O. Bossen, and A. Amato, *Phys. Rev. Lett.* **106**, 117602 (2011).
- [11] F. Ye, S. Chi, W. Bao, X. F. Wang, J. J. Ying, X. H. Chen, H. D. Wang, C. H. Dong, and M. Fang, *Phys. Rev. Lett.* **107**, 137003 (2011).
- [12] H. Hong and H. Steinfink, *J. Solid State Chem.* **5**, 93 (1972).
- [13] A. Krzton-Maziopa, E. Pomjakushina, V. Pomjakushin, D. Sheptyakov, D. Chernyshov, V. Svitlyk, and K. Conder, *J. Phys.: Condens. Matter* **23**, 402201 (2011).
- [14] J. M. Caron, J. R. Neilson, D. C. Miller, A. Llobet, and T. M. McQueen, *Phys. Rev. B* **84**, 180409 (2011).
- [15] J. M. Caron, J. R. Neilson, D. C. Miller, K. Arpino, A. Llobet, and T. M. McQueen, *Phys. Rev. B* **85**, 180405 (2012).
- [16] Y. Nambu, K. Ohgushi, S. Suzuki, F. Du, M. Avdeev, Y. Uwatoko, K. Munakata, H. Fukazawa, S. Chi, Y. Ueda, and T. J. Sato, *Phys. Rev. B* **85**, 064413 (2012).
- [17] F. Du, K. Ohgushi, Y. Nambu, T. Kawakami, M. Avdeev, Y. Hirata, Y. Watanabe, T. J. Sato, and Y. Ueda, *Phys. Rev. B* **85**, 214436 (2012).
- [18] S. Chi, Y. Uwatoko, H. Cao, Y. Hirata, K. Hashizume, T. Aoyama, and K. Ohgushi, *Phys. Rev. Lett.* **117**, 047003 (2016).
- [19] H. Takahashi, A. Sugimoto, Y. Nambu, T. Yamauchi, Y. Hirata, T. Kawakami, M. Avdeev, K. Matsubayashi, F. Du, C. Kawashima, H. Soeda, S. Nakano, Y. Uwatoko, Y. Ueda, T. J. Sato, and K. Ohgushi, *Nat. Mater.* **14**, 1008 (2015).
- [20] T. Yamauchi, Y. Hirata, Y. Ueda, and K. Ohgushi, *Phys. Rev. Lett.* **115**, 246402 (2015).
- [21] H. Lei, H. Ryu, A. I. Frenkel, and C. Petrovic, *Phys. Rev. B* **84**, 214511 (2011).
- [22] Y. Hirata, S. Maki, J. I. Yamaura, T. Yamauchi, and K. Ohgushi, *Phys. Rev. B* **92**, 205109 (2015).
- [23] C. Monney, A. Uldry, K. J. Zhou, A. Krzton-Maziopa, E. Pomjakushina, V. N. Strocov, B. Delley, and T. Schmitt, *Phys. Rev. B* **88**, 165103 (2013).
- [24] D. Ootsuki, N. L. Saini, F. Du, Y. Hirata, K. Ohgushi, Y. Ueda, and T. Mizokawa, *Phys. Rev. B* **91**, 014505 (2015).
- [25] Q. Luo, A. Nicholson, J. Rincon, S. Liang, J. Riera, G. Alvarez, L. Wang, W. Ku, G. D. Samolyuk, A. Moreo, and E. Dagotto, *Phys. Rev. B* **87**, 024404 (2013).
- [26] S. Dong, J.-M. Liu, and E. Dagotto, *Phys. Rev. Lett.* **113**, 187204 (2014).
- [27] Z. V. Popović, M. Šćepanovic, N. Lazarević, M. Opačić, M. M. Radonjić, D. Tanasković, H. Lei, and C. Petrovic, *Phys. Rev. B* **91**, 064303 (2015).
- [28] K. Homma and F. Izumi, *J. Appl. Crystallogr.* **44**, 1272 (2011).
- [29] R. M. Fernandes, A. V. Chubukov, and J. Schmalian, *Nat. Phys.* **10**, 97 (2014).
- [30] J.-H. Chu, J. G. Analytis, K. De Greve, P. L. McMahon, Z. Islam, Y. Yamamoto, and I. R. Fisher, *Science* **329**, 824 (2010).
- [31] J. J. Ying, X. F. Wang, T. Wu, Z. J. Xiang, R. H. Liu, Y. J. Yan, A. F. Wang, M. Zhang, G. J. Ye, P. Cheng, J. P. Hu, and X. H. Chen, *Phys. Rev. Lett.* **107**, 067001 (2011).
- [32] J.-H. Chu, H.-H. Kuo, J. G. Analytis, and I. R. Fisher, *Science* **337**, 710 (2012).
- [33] A. Dusza, A. Lucarelli, F. Pfuner, J.-H. Chu, I. R. Fisher, and L. Degiorgi, *Europhys. Lett* **93**, 37002 (2011).
- [34] M. Yi, D. Lu, J.-H. Chu, J. Analytis, A. Sorini, A. Kemper, B. Moritz, S.-K. Mo, R. G. Moore, M. Hashimoto, W.-S. Lee, Z. Hussain, T. Devereaux, I. R. Fisher, and Z.-X. Shen, *Proc. Natl. Acad. Sci. USA* **108**, 6878 (2011).
- [35] Y. K. Kim, W. S. Jung, G. R. Han, K.-Y. Choi, C.-C. Chen, T. P. Devereaux, A. Chainani, J. Miyawaki, Y. Takata, Y. Tanaka, M. Oura, S. Shin, A. P. Singh, H. G. Lee, J.-Y. Kim, and C. Kim, *Phys. Rev. Lett.* **111**, 217001 (2013).
- [36] D. G. Hawthorn, F. He, L. Venema, H. Davis, A. J. Achkar, J. Zhang, R. Sutarto, H. Wadati, A. Radi, T. Wilson, G. Wright, K. M. Shen, J. Geck, H. Zhang, V. Novk, and G. A. Sawatzky, *Rev. Sci. Instrum.* **82**, 073104 (2011).
- [37] N. L. Saini, Y. Wakisaka, B. Joseph, A. Iadecola, S. Dalela, P. Srivastava, E. Magnano, M. Malvestuto, Y. Mizuguchi, Y. Takano, T. Mizokawa, and K. B. Garg, *Phys. Rev. B* **83**, 052502 (2011).
- [38] W. L. Yang, A. P. Sorini, C.-C. Chen, B. Moritz, W.-S. Lee, F. Vernay, P. Olalde-Velasco, J. D. Denlinger, B. Delley, J.-H. Chu, J. G. Analytis, I. R. Fisher, Z. A. Ren, J. Yang, W. Lu, Z. X. Zhao, J. van den Brink, Z. Hussain, Z.-X. Shen, and T. P. Devereaux, *Phys. Rev. B* **80**, 014508 (2009).

- [39] C. Parks Cheney, F. Bondino, T. A. Callcott, P. Vilmercati, D. Ederer, E. Magnano, M. Malvestuto, F. Parmigiani, A. S. Sefat, M. A. McGuire, R. Jin, B. C. Sales, D. Mandrus, D. J. Singh, J. W. Freeland, and N. Mannella, *Phys. Rev. B* **81**, 104518 (2010).
- [40] F. Bondino, E. Magnano, M. Malvestuto, F. Parmigiani, M. A. McGuire, A. S. Sefat, B. C. Sales, R. Jin, D. Mandrus, E. W. Plummer, D. J. Singh, and N. Mannella, *Phys. Rev. Lett.* **101**, 267001 (2008).
- [41] F. Bondino, E. Magnano, C. H. Booth, F. Offi, G. Panaccione, M. Malvestuto, G. Paolicelli, L. Simonelli, F. Parmigiani, M. A. McGuire, A. S. Sefat, B. C. Sales, R. Jin, P. Vilmercati, D. Mandrus, D. J. Singh, and N. Mannella, *Phys. Rev. B* **82**, 014529 (2010).
- [42] C.-C. Chen, J. Maciejko, A. P. Sorini, B. Moritz, R. R. P. Singh, and T. P. Devereaux, *Phys. Rev. B* **82**, 100504(R) (2010).
- [43] R. Arita, H. Ikeda, S. Sakai, and M.-T. Suzuki, *Phys. Rev. B* **92**, 054515 (2015).
- [44] M.-T. Suzuki, R. Arita, and H. Ikeda, *Phys. Rev. B* **92**, 085116 (2015).
- [45] V. Pardo, S. Blanco-Canosa, F. Rivadulla, D. I. Khomskii, D. Baldomir, Hua Wu, and J. Rivas, *Phys. Rev. Lett.* **101**, 256403 (2008).
- [46] I. I. Mazin, H. O. Jeschke, K. Foyevtsova, R. Valenti, and D. I. Khomskii, *Phys. Rev. Lett.* **109**, 197201 (2012).
- [47] M. Wang, S. J. Jin, M. Yi, Y. Song, H. C. Jiang, W. L. Zhang, H. L. Sun, H. Q. Luo, A. D. Christianson, E. Bourret-Courchesne, D. H. Lee, D.-X. Yao, and R. J. Birgeneau, *Phys. Rev. B* **95**, 060502(R) (2017).
- [48] K. Haule and G. Kotliar, *New J. Phys.* **11**, 025021 (2009).